Mechanism of Nucleocapsid Protein Catalyzed Structural Isomerization of the Dimerization Initiation Site of HIV-1†

Manuela J. Rist‡ and John P. Marino*

Center for Advanced Research in Biotechnology of the University of Maryland and the National Institute for Standards and Technology, 9600 Gudelsky Drive, Rockville, Maryland 20850

Received August 24, 2002; Revised Manuscript Received October 8, 2002

ABSTRACT: Dimerization of two homologous strands of genomic RNA is an essential feature of retroviral replication. In the human immunodeficiency virus type 1 (HIV-1), a conserved stem−loop sequence, the dimerization initiation site (DIS), has been identified as the domain primarily responsible for initiation of this aspect of viral assembly. The DIS loop contains an autocomplementary hexanucleotide sequence flanked by highly conserved 5′ and 3′ purines and can form a homodimer through a loop−loop kissing interaction. In a structural rearrangement activated by the HIV-1 nucleocapsid protein (NCp7) and considered to be associated with viral particle maturation, the DIS dimer converts from an intermediate kissing to an extended duplex isoform. Using 2-aminopurine (2-AP) labeled sequences derived from the DIS_{Mal} variant and fluorescence methods, the two DIS dimer isoforms have been unambiguously distinguished, allowing a detailed examination of the kinetics of this RNA structural isomerization and a characterization of the role of NCp7 in the reaction. In the presence of divalent cations, the DIS kissing dimer is found to be kinetically trapped and converts to the extended duplex isoform only upon addition of NCp7. NCp7 is demonstrated to act catalytically in inducing the structural isomerization by accelerating the rate of strand exchange between the two hairpin stem helices, without disruption of the loop−loop helix. Observation of an apparent maximum conversion rate for NCp7-activated DIS isomerization, however, requires protein concentrations in excess of the 2:1 stoichiometry estimated for high-affinity NCp7 binding to the DIS kissing dimer, indicating that transient interactions with additional NCp7(s) may be required for catalysis.

All known retroviruses package two identical positive copies of their RNA genomes into budding viral particles that are linked noncovalently through a leader sequence at the 5′ end of the RNA genome termed the dimer linkage structure (DLS)[1] (*1*−*3*). RNA genome dimerization is proposed to be involved in a number of important events in the retroviral life cycle, including recombination and reverse transcription (*1*), translation of the *gag* gene (*4*), and selective encapsidation and packaging of genomic RNA (*5*−*11*). In the human immunodeficiency virus type-1 (HIV-1), dimerization is initiated by a highly conserved 35-nucleotide stem−loop, called the dimerization initiation site (DIS), which is located within the DLS (*7*, *12*−*16*). Deletion or mutation of the DIS sequence has been found to dramatically decrease viral replication rates and reduce infectivity by as much as 1000-fold (*1*, *7*, *9*, *10*) with specific defects shown to effect genomic RNA dimerization and encapsidation as well as proviral DNA synthesis (*7*, *9*, *10*, *14*, *17*, *18*). The DIS loop contains an autocomplementary hexanucleotide sequence, which is found most often to be either GUGCAC (subtype A or Mal variant) or GCGCGC (subtype B or Lai variant), together with highly conserved 5′ and 3′ flanking purine nucleotides (Figure 1A). In vitro experiments have shown that sequences derived from the DLS can spontaneously form stable homodimers under certain ionic conditions through a loop−loop kissing interaction and that isolated DIS stem−loops will also self-associate to form kissing homodimers (*1*, *8*, *16*, *19*−*25*).

After the HIV-1 virus is released from the cell, the retroviral RNA homodimer undergoes conformational changes that result in the formation of a more compact, thermodynamically stable dimer (*26*, *27*). This so-called "maturation" of the post-budded retroviral RNA genome requires active viral protease and appears to correlate with cleavage of the nucleocapsid protein (NCp7) from *gag* in the viral particle. It has been suggested that the released NCp7 acts as a nucleic acid chaperone (*28*) by activating RNA refolding events associated with genomic RNA maturation. Strong evidence of such a catalytic role for NCp7 in the genomic RNA dimer maturation process has been provided by in vitro studies, which demonstrated that NCp7 activates conversion of metastable homodimers formed either between short retroviral RNA transcripts from the 5′ end of Harvey sarcoma virus or between the Lai subtype of HIV-1 to more stable mature dimer forms (*29*, *30*). In further in vitro studies with the Lai sequence variant of HIV-1, the DIS kissing dimer has been shown to be converted under certain ionic conditions by incubation either at 55 °C or with the addition of

† This work was supported by the NIH (GM 59107) to J.P.M.

* Corresponding author telephone: (301)738-6160; fax: (301)738-6255; e-mail: marino@carb.nist.gov.

‡ Present address: Institut für Organische Chemie und Biochemie II der TU München, Lichtenbergstrasse 4, D-85747 Garching, Germany.

[1] Abbreviations: DLS, dimerization linkage structure; HIV-1, human immune deficiency virus type 1; DIS, dimerization initiation site; NCp7, nucleocapsid protein; PBS, primer binding site; 2-AP, 2-aminopurine; PAGE, polyacrylamide gel electrophoresis.

10.1021/bi0267240 CCC: $22.00
Published on Web 11/15/2002

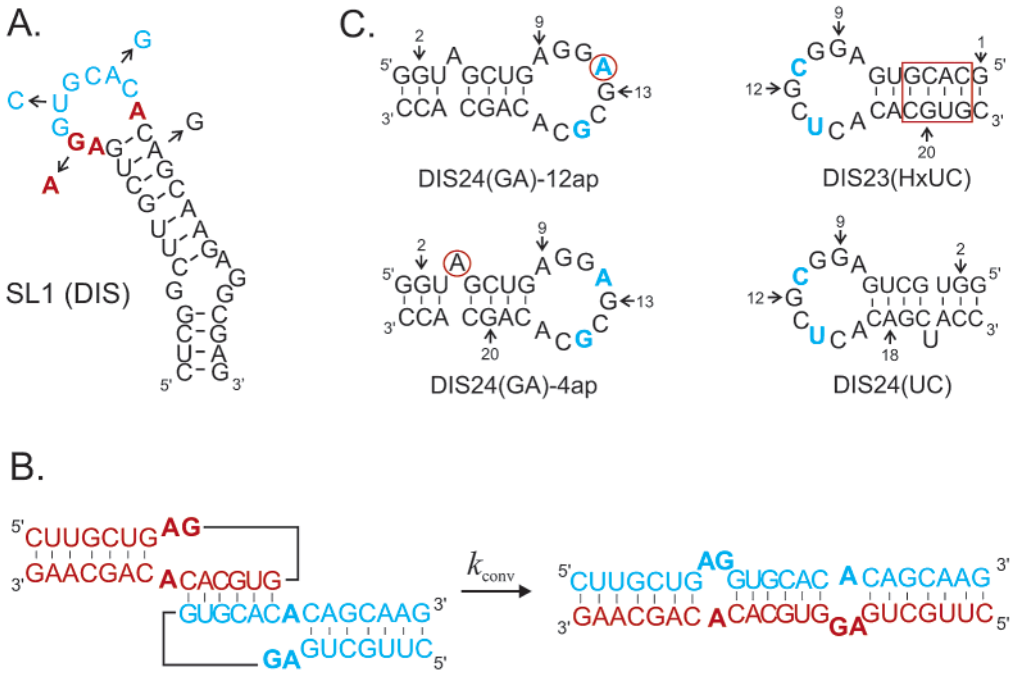

FIGURE 1: (A) RNA sequence and secondary structure of the DIS (SL1) stem−loop from subtype-A of HIV-1. In the DIS loop, the hexanucleotide palindrome sequence is highlighted in blue, and conserved flanking purine nucleotides are bolded in red. Positions in the sequences that differ for the subtype-B strain of HIV-1 are indicated by arrows and substituted nucleotides. (B) Schematic of the structural conversion of the DIS homodimer from loop−loop kissing to extended duplex conformations. In each of the two dimers, one of the two identical hairpin sequences is shown in red and the other is in blue. (C) RNA sequence and secondary structure of the DIS stem−loop constructs designed to form heterodimer complexes. Point mutations in the hexanucleotide sequence [U12→A12 and A15→G15 to form the DIS(GA) stem−loop and U11→C11 and A14→U14 to form the complementary DIS(UC) stem−loop] that destroy the palindromic nature of the sequence and promote heterodimer formation are bolded in blue. Nucleotide positions in the DIS(GA) stem−loop that were substituted with the fluorescent probe 2-AP are circled in red. The exchanged stem helix of DIS23(HxUC) is boxed in red.

NCp7 at 37 °C to a more thermodynamically stable extended duplex dimer form as shown in Figure 1B (*16*, *31*−*35*). This NCp7 activated structural isomerization of DIS observed in vitro has been suggested to be related to the process of RNA genome maturation in budding viral particles. NCp7 has also been shown to act as a nucleic acid chaperone in promoting a number of other nucleic acid annealing and strand transfer processes involved in HIV-1 replication, such as $tRNA^{Lys}$ hybridization to the primer binding site (PBS) on genomic RNA (*36*−*38*) and strand transfer and renaturation reactions after the initiation of reverse transcription (*39*−*48*).

High-resolution structures of the DIS kissing and mature duplex dimer forms from both HIV-1 Mal and Lai variants have been determined through solution NMR (*49*−*51*) and crystallographic (*52*, *53*) methods. To date, however, a number of unresolved discrepancies exist between the solution and the X-ray determined structures. In addition, mechanisms for the DIS dimer structural isomerization and the specific role of NCp7 in this reaction that have been proposed on the basis of these structural studies have only been speculative. In this study, fluorescence-detected methods have been used to determine the molecular mechanism of HIV-1 DIS structural isomerization and to address the specific role of NCp7 in the process. The highly fluorescent nucleotide base analogue 2-aminopurine (2-AP) has been incorporated as a structural probe at specific positions in stem−loop sequences derived from the wild-type DIS_{Mal} sequence (Figure 1C). As shown in previous studies of RNA interactions with proteins, peptides, and small ligands (*54*−*58*), the quantum yield of 2-AP fluorescence emission is extremely sensitive to its microenvironment and thus can act as an ideal reporter of changes in RNA structure, dynamics, and intermolecular interactions. Here, the 2-AP labeled DIS stem−loops have been designed to provide unambiguous and specific fluorescence probes for formation of each of the two isoforms of the DIS_{Mal} dimer. Using the 2-AP labeled DIS stem−loops, equilibrium and kinetic binding constants for DIS dimerization as well as NCp7 activated rates of DIS structural isomerization have been measured.

MATERIALS AND METHODS[2]

RNA and NCp7 Sample Preparation. 2-Aminopurine 2′-*O*-methylriboside containing RNA oligonucleotides (Figure 1C) were synthesized on an Applied Biosystems 390 synthesizer (Perkin-Elmer, Forest City, CA) using standard phosphoramidite chemistry (*59*) with nucleoside phophoramidites purchased from Glen Research (Sterling, VA). Synthesized RNA oligonucleotides were deprotected using standard protocols. Unlabeled RNA oligonucleotides were prepared by in vitro T7 polymerase runoff transcription using synthetic DNA templates according to the method of Milligan and co-workers (*60*, *61*). All RNA oligonucleotides were purified using preparative-scale denaturing polyacrylamide gel electrophoresis (PAGE), recovered by electrophoretic elution, and then desalted and exchanged into standard buffer

[2] Certain commercial equipment, instruments, and materials are identified in this paper in order to specify the experimental procedure. Such identification does not imply recommendation or endorsement by the National Institute of Standards and Technology, nor does it imply that the material or equipment identified is necessarily the best available for the purpose.

(1 mM cacodylate [pH 6.5], 25 mM NaCl) through extensive dialysis using a microdialysis system (Pierce Instruments, Rockford, IL). The NCp7 protein was expressed and purified as described previously (*62*).

For this study, the palindromic hexanucleotide DIS loop sequence of the Mal variant has been altered to create two unique DIS stem−loops (Figure 1C), so-called DIS(GA) and DIS(UC), which associate at nanomolar concentrations as heterodimers rather than homodimers. This method of creating heterodimers through loop sequence alteration has previously been demonstrated for the DIS Lai variant (*8*, *33*). 2-AP labels were inserted at two specific positions in the DIS24(GA) stem−loop: one construct with 2-AP substituted at the A12 loop position [DIS24(GA)-12ap] and a second with 2-AP inserted as a single bulged nucleotide in the stem [DIS24(GA)-4ap]. These two constructs were designed to probe kissing versus mature duplex dimer formation, respectively. Two unlabeled DIS(UC) constructs with hexanucleotide loop sequences complementary to the DIS24(GA) stem−loops have also been designed: one construct with a stem sequence complementary to DIS24-(GA)-4ap that can specifically probe the DIS structural isomerization [DIS24(UC)] and a second construct with an exchanged stem sequence that is capable of forming only the kissing dimer [DIS23(HxUC)].

Fluorescence Detection of DIS Kissing Dimer Formation and Binding by NCp7. The fluorescence emission spectra of RNA oligonucleotide samples (100 nM) selectively labeled with 2-AP were measured on a SPEX Fluoromax-2 spectrofluorometer (Instruments SA, Edison, NJ) using a 0.3 cm square cuvette in 150 μL of standard buffer solution with 5 mM $MgCl_2$. Emission spectra were recorded over the wavelength range of 330−450 nm with an excitation wavelength of 310 nm and a spectral band-pass of 5 nm. The equilibrium binding constant (K_D) for DIS loop−loop kissing dimer formation was determined at 25 °C by following the decrease in fluorescence at 371 nm as a fixed concentration of the fluorescent DIS24(GA)-12ap was titrated with increasing amounts of either the DIS24(UC) or the DIS23(HxUC) complement. The RNA−RNA interaction in each case was fit using a single-site equilibrium binding equation. For example, single-site binding of DIS24(UC) to DIS24(GA)-12ap was fit using eq 1 as follows:

$$F = -\{(F_0 - F_f)/2[\text{DIS24(GA)}]_{tot}\} \times \left\{b - \sqrt{b^2 - 4[\text{DIS24(UC)}]_{tot}[\text{DIS24(GA)}]_{tot}}\right\} + F_0 \quad (1)$$
$$b = K_d + [\text{DIS24(UC)}]_{tot} + [\text{DIS24(GA)}]_{tot}$$

where F_0 and F_f are the initial and final fluorescence intensities, respectively; $[\text{DIS24(GA)}]_{tot}$ is the total DIS24-(GA)-12ap concentration; and $[\text{DIS24(UC)}]_{tot}$ is the total concentration of DIS24(UC).

The dissociation kinetics of the DIS loop−loop kissing dimer was measured by following the increase in 2-AP fluorescence of DIS24(GA)-12ap over time as the DIS24-(GA)-12ap•DIS23(HxUC) complex dissociates. The reaction was carried out at 35 °C using a DIS kissing dimer concentration of 100 nM in standard buffer solution with 5 mM $MgCl_2$ and made irreversible by trapping the free DIS23-(HxUC) with a 20-fold excess of unlabeled DIS24(GA) stem−loop added manually. For dissociation experiments carried out in the presence of NCp7, the DIS24(GA)-12ap•DIS23(HxUC) kissing dimer was preincubated with 500 nM protein. The time course of the dissociation of the DIS kissing dimer was fit using the first-order rate equation, $F_t = F_1[1 - \exp(-k_1 t)] + C$, where F_1 and k_1 are the amplitude and observed off-rate, respectively, for the complex and C is a constant offset.

The kinetics of RNA−RNA association was followed at 25 °C in standard buffer solution with 5 mM $MgCl_2$ using pseudo-first-order conditions where DIS23(HxUC) was present at concentrations of 20-fold greater than the DIS24-(GA)-12ap. A DIS24(GA)-12ap concentration of 100 nM was used. For association experiments carried out in the presence of NCp7, DIS23(HxUC) was preincubated with 500 nM protein, and the two macromolecules were mixed simultaneously with DIS24(GA)-12ap. The time course of the decrease in 2-AP fluorescence (F_t) as a result of loop−loop complex formation was fit using the first-order rate equation, $F_t = F_1 \exp(-k_1 t) + C$ where F_1 and k_1 are the amplitude and apparent on-rate, respectively, for the complex and C is a constant offset.

Binding of NCp7 to the DIS kissing dimer was followed by monitoring the quenching of tryptophan fluorescence emission as a fixed concentration (250 or 500 nM) of NCp7 was titrated with increasing amounts of a preformed DIS kissing complex. Tryptophan fluorescence emission was recorded over the wavelength range of 310−450 nm, with an excitation wavelength of 295 nm and a spectral band-pass of 5 nm. NCp7 binding was fit using eq 2, assuming two equivalent sites for NCp7 on the DIS kissing dimer as follows:

$$F = -\{(F_0 - F_f)/2[\text{DIS Kiss}]_{2tot}\} \times \left\{b - \sqrt{b^2 - 4[\text{NCp7}]_{tot}[\text{DIS Kiss}]_{2tot}}\right\} + F_0 \quad (2)$$
$$b = K_d + [\text{NCp7}]_{tot} + [\text{DIS Kiss}]_{2tot}$$

where F_0 and F_f are the initial and final fluorescence intensities, respectively; $[\text{DIS Kiss}]_{2tot}$ is twice the total DIS-(AG)•DIS(UC) complex concentration; and $[\text{NCp7}]_{tot}$ is the total concentration of NCp7 protein.

Kinetic Measurement of NCp7-Catalyzed Structural Isomerization of the DIS Dimer. NCp7-catalyzed structural isomerization of DIS was measured at 25 °C using the SPEX Fluoromax-2 spectrofluorometer by following the decrease in fluorescence emission over time as the DIS24(GA)-4ap•DIS24(UC) kissing dimer is converted to the extended duplex. In all experiments, the DIS24(GA)-4ap•DIS24(UC) kissing dimer was first formed in standard buffer solution with 5 mM $MgCl_2$, then mixed manually with NCp7, and rapidly inserted into the spectrofluorometer for fluorescence measurements. Because of the relatively slow DIS conversion rates, the kinetic resolution of a few seconds afforded by manual mixing was sufficient to obtain reasonably accurate rate measurements. The time course of the conversion of the DIS kissing dimer was fit using the first-order rate equation, $F_t = F_1 \exp(-k_{conv} t) + C$, where k_{conv} is the observed isomerization rate for conversion of DIS kissing to extended mature duplex dimer. Other specific conditions for individual experiments are described in the figure legends and text.

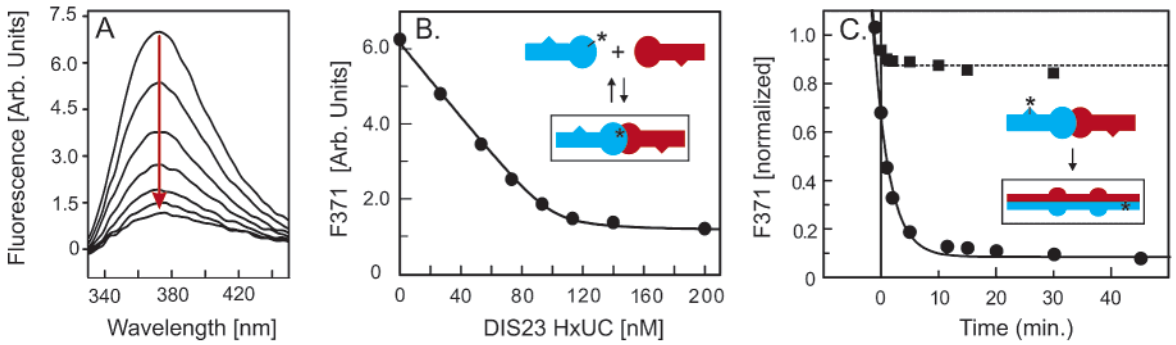

FIGURE 2: (A) Fluorescence changes accompanying titration of 100 nM DIS24(GA)-12ap with increasing concentrations of DIS23(HxUC) in standard buffer with 5 mM $MgCl_2$ at 25 °C. Emission spectra are plotted from 330 to 450 nm. (B) Plot of the fluorescence decrease at 371 nm as a function of total DIS23(HxUC) concentration for a titration using 100 nM DIS24(GA)-12ap. The location of the 2-AP probe on the DIS(GA) stem−loop is indicated by an asterisk, and the species that is directly detected in the experiment is marked with a box in the panel. The solid curve is fit ($K_D = 1.3 \pm 0.7$ nM) using a single-site equilibrium binding equation. (C) Plot of the fluorescence decrease at 371 nm (filled circles) as a function of time after a 2.5-fold excess of NCp7 protein is added to 100 nM DIS24(GA)-4ap•DIS24(UC) kissing complex preformed in the presence of 5 mM $MgCl_2$. The location of the 2-AP probe on the DIS(GA) stem−loop is indicated by an asterisk, and the species that is directly detected in the experiment is marked with a box in the panel. The structural isomerization rate was fit using a first-order rate constant equation ($k_{conv} = 0.46$ min^{-1}). A similar experiment with the preformed DIS24(GA)-4ap•DIS23-(HxUC) complex resulted in only a 10% initial decrease in fluorescence (filled squares and dashed line).

RESULTS

Using 2-AP labeled DIS stem−loops, equilibrium and kinetic binding constants for the DIS loop−loop kissing dimer were determined. Titration of the DIS_{Mal}-derived hairpin, DIS24(GA)-12ap, substituted with 2-AP at position A12 in the loop (Figure 1C) with either of the complementary DIS(UC) stem−loops [DIS24(UC) or DIS23(HxUC)], results in an approximately 6-fold decrease in 2-AP fluorescence emission (Figure 2A,B). The direction and magnitude of this fluorescence change indicates that the 2-AP-substituted base becomes significantly stacked upon binding, which is consistent with 2-AP•U base pairing that would accompany the formation of the DIS kissing complex loop−loop helix. A similar quenching effect of loop-substituted 2-AP probes has previously been observed upon formation of kissing complexes between RNA stem−loops derived from antisense RNAs associated with *ColE1* plasmid replication control (*58*). Using 2-AP fluorescence quenching measurements, the heterodimeric DIS kissing complexes were found to have equilibrium binding constants (average $K_D = 3 \pm 1$ nM), which were consistent with previous measurements made using other techniques (*22*−*25*). A comparable binding affinity was determined for the entire 35-nucleotide DIS stem−loop using similar fluorescence quenching measurements, leading to the conclusion that the stem structure does not have a significant effect on the DIS kissing dimer association and that the presence of a stem bulge found in wild-type DIS is not required. These truncated DIS stem−loops therefore faithfully mimic the kissing association of the wild-type 35-nucleotide DIS stem−loop and provide a useful in vitro system for modeling this interaction.

To unambiguously detect the DIS structural isomerization and to determine the role of NCp7 in this process, the stem−loop DIS24(GA)-4ap capable of forming heterodimeric DIS24(GA)•DIS24(UC) complexes was constructed with a 2-AP probe inserted into the stem sequence such that it formed a single nucleotide bulge (Figure 1C). The fluorescence of the 2-AP probe at this position in the free DIS24-(GA) stem−loop was found to be relatively high and confirmed that the 2-AP is indeed in an unpaired bulged state. Upon formation of a DIS kissing dimer with the DIS24-(UC) stem−loop in standard buffer containing 5 mM $MgCl_2$, the fluorescence intensity of the 2-AP probe of DIS24(GA)-4ap was found to initially increase slightly (∼25%) but then remained constant. If the DIS dimer formed represented the mature duplex dimer rather than the kissing dimer or if the mature dimer state became populated with time, a significant quench of fluorescence emission of the 2-AP probe in DIS24-(GA)-4ap would have been expected as a result of the formation and stacking of a 2-AP•U base pair between the 2-AP base from DIS24(GA)-4ap and the single-stem bulged uridine of DIS24(UC) in the mature dimer. The Mg^{2+}-stabilized DIS kissing dimers are therefore kinetically trapped, as has been observed for kissing complexes associated with regulatory RNAs involved in regulation of plasmid replication in bacteria (*63*, *64*). In contrast to the bacterial RNA systems, the DIS stem−loops were also observed to associate as kissing dimers in the presence of monovalent cations, such as Na^+ or K^+ in concentrations of 100−300 mM or with sufficiently high RNA concentrations (> μM) under standard buffer conditions. DIS kissing dimers formed under these conditions, however, have been found to be metastable and capable of spontaneously converting to the mature duplex form at an appreciable rate over time (data not shown).

To determine the effect of NCp7 on the isomerization of Mg^{2+}-stabilized DIS kissing dimers, NCp7 was added directly to DIS kissing complexes preformed between the DIS24(GA)-4ap and the complementary DIS24(UC) stem−loops, and the fluorescence emission of the 2-AP reported in the DIS24(GA)-4ap stem−loop was monitored. As mentioned above, since the DIS24(UC) stem−loop contains a single stem bulged uridine that can form a 2-AP•U base pair in the mature duplex dimer with the 2-AP base from DIS24(GA)-4ap, the environment of the reporter 2-AP is expected to change from a bulged, highly fluorescent state in the kissing dimer to a stacked, quenched state in the mature dimer, assuming that the stem strands are exchanged during the reaction. As shown in Figure 2C, a time-dependent 5-fold decrease in 2-AP fluorescence emission is observed in the experiment. The direction and magnitude of the observed fluorescence change indicates that the 2-AP-substituted base

does become significantly stacked with time, which is consistent with 2-AP•U base pairing and stacking that would accompany exchange of the stem strands during the isomerization process. To confirm that the change in fluorescence observed is due to DIS structural conversion and exchange of stem strands, the fluorescence response of NCp7 addition to a kissing complex formed between DIS24(GA)-4ap and DIS23(HxUC), which contains a mismatched stem sequence incapable of forming proper Watson−Crick base pairs in the mature duplex dimer, was measured. Although the DIS23-(HxUC) stem−loop efficiently forms a kinetically stable kissing dimer with DIS24(GA)-4ap in the presence of 5 mM Mg^{2+}, time-dependent quenching of the stem 2-AP probe was not observed when NCp7 was added to catalyze conversion of this DIS kissing dimer (Figure 2C). Instead, only an initial static decrease (∼10%) in the fluorescence of the 2-AP probe was observed. Addition of Mg^{2+} directly to the individual DIS24(GA)-4ap stem−loop also resulted in only a slight static increase in the 2-AP fluorescence emission (25%), further confirming that direct interaction of neither NCp7 nor Mg^{2+} with the 2-AP label is responsible for the observed temporal changes in the 2-AP fluorescence emission. Thus, strand exchange of the stem helices associated with DIS structural isomerization is clearly the source of the quenching of 2-AP fluorescence in the experiment.

To further elucidate the role of NCp7 in the DIS dimer isomerization, the importance of preformation of the DIS kissing dimer structure in specific NCp7 binding and activity was examined using antisense oligonucleotide probes (Figure 3A). DIS conversion rates were measured essentially as described above in the presence of a 10-fold excess of either 6-mer or 7-mer antisense DNA oligonucleotides complementary to the central DIS(GA) loop sequence. These antisense oligonucleotides compete with DIS(UC) for binding to DIS(GA) and thereby slow the rate of DIS(GA)•DIS(UC) kissing association (*22*). At a 10-fold excess concentration, saturated binding of the oligonucleotides to the DIS(GA) loop is observed (data not shown). If preformation of the DIS kissing dimer structure is important for NCp7-activated isomerization, the addition of the antisense DNA oligonucleotide competitors directed at the DIS(GA) loop sequence would be expected to slow the rate of conversion. In the presence of these antisense oligonucleotides, the rate of the NCp7-catalyzed conversion of the DIS kissing complex to mature duplex is reduced as would be expected based on this model of competitive inhibition of kissing association (Figure 3A). Thus, preformation of the DIS kissing dimer appears to be required for rapid, NCp7-catalyzed structural isomerization. In contrast, a 10-fold excess of a 7-mer DNA oligonucleotide designed to bind competitively to the stem of DIS(GA) did not significantly affect the rate of conversion (Figure 3A). This result indicates that, although the stem strands are exchanged during the conversion reaction, the lifetime of any single-stranded species is not long enough to allow capture by the antisense competitor. It also demonstrates that the reduction in rate of isomerization by the antisense DNA competitors is not related to inhibition due to direct competitive binding of the oligonucleotides with NCp7, which is known to bind both single-stranded RNA and DNA oligonucleotides with micromolar affinity (*65*, *66*).

The effect of NCp7 on the dissociation and association rates of the DIS kissing dimer has also been examined

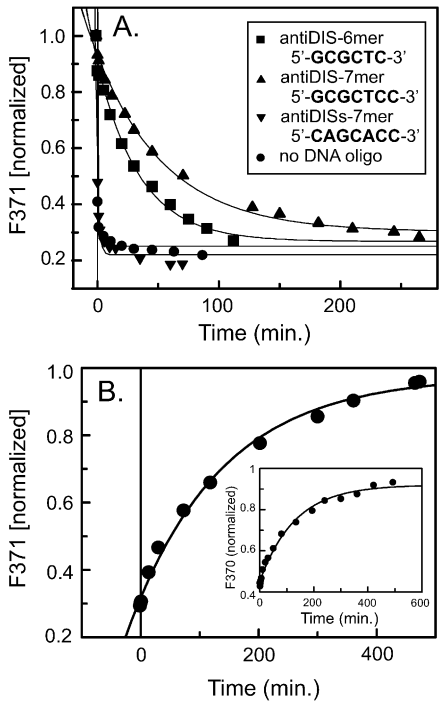

FIGURE 3: (A) Plot of the rate of structural isomerization of the kissing complex to mature duplex in the presence of antisense 7-mer (filled triangles) and 6-mer (filled squares) DNA oligonucleotides complementary to the DIS(GA) loop sequence, in the presence of a 7-mer DNA oligonucleotide (filled inverted triangles) complementary to a strand of the DIS(GA) stem and in the absence of any DNA competitors (filled circles). Solid lines show the rates for the structural isomerization that were fit using a first-order rate constant equation [antisense-6-mer: $k_{conv} = 0.029 \pm 0.004$ min^{-1}; antisense-7-mer: $k_{conv} = 0.018 \pm 0.002$ min^{-1}; stem−7-mer and no DNA competitor: $k_{conv} \geq 0.55 \pm 0.04$ min^{-1}]. (B) Kinetic measurement of the DIS loop−loop kissing complex dissociation. Fluorescence change upon rapid mixing of DIS24(GA)-12ap•DIS23-(HxUC) with excess (2 μM) unlabeled DIS24(GA) acting as an irreversible trap for the free DIS23(HxUC). The data were fit ($k_{off} = 1.05 \times 10^{-4}$ s^{-1}) using a first-order rate equation. In a similar experiment that is plotted in the inset, the k_{off} for DIS24(GA)-12ap from DIS23(HxUC) was determined with 500 nM NCp7 present in the buffer ($k_{off} = 1.08 \times 10^{-4}$ s^{-1}).

(Figure 3B and data not shown). The dissociation kinetics of the DIS loop−loop kissing dimer was measured by following the increase in 2-AP fluorescence of DIS24(GA)-12ap as the DIS24(GA)-12ap•DIS23(HxUC) complex dissociates and made irreversible by trapping the free DIS23-(HxUC) with a 20-fold excess of unlabeled DIS24(GA) stem−loop. An apparent on-rate for DIS complex formation was followed using pseudo-first-order conditions, where a 20-fold greater concentration of DIS23(HxUC) was added to DIS24(GA)-12ap. In both association and dissociation measurements, it was found that addition of NCp7 to the reaction mixture did not significantly affect the observed kinetic rates. In addition, no significant increase in the intensity of the fluorescence emission of the DIS(GA)-12ap probe within the DIS kissing loop−loop helix is observed as a function of DIS conversion. This indicates that the 2-AP base remains well-stacked during the DIS structural isomerization and suggests that the integrity of the loop−loop kissing helix is not significantly perturbed during the process. Taken together, these results indicate that NCp7 recognizes and binds to a preformed DIS kissing dimer and catalyzes isomerization, while the dimeric nature

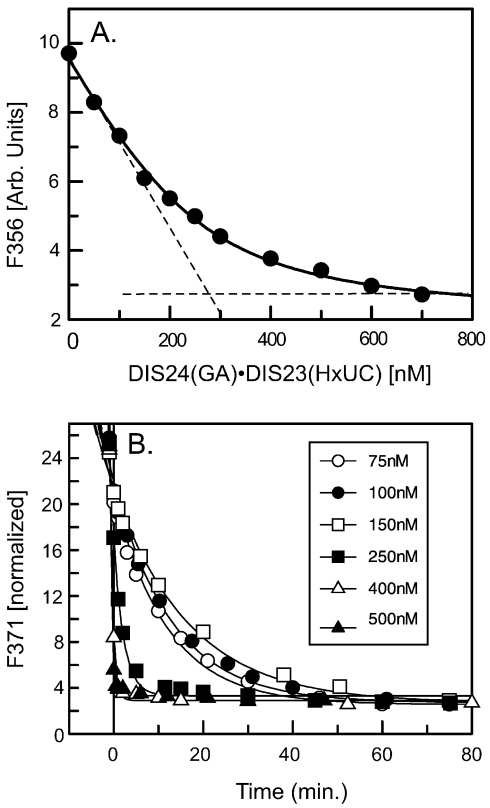

FIGURE 4: (A) Plot of the decrease in fluorescence at 356 nm as a result of titration of 500 nM NCp7 with a preformed DIS24-(GA)•DIS23(HxUC) complex [RNA complex was in standard buffer containing 5 mM $MgCl_2$]. The solid curve is fit ($K_D = 61 \pm 12$ nM) using an equilibrium binding equation and assuming two equivalent binding sites for NCp7. A linear extrapolation of the first few points is shown as a dashed line. The *x*-intercept of this line gives an estimated binding stoichiometry of 2:1 (NCp7:DIS dimer). Binding data were collected at 25 °C. (B) Plots of the rate of structural isomerization of 100 nM DIS24(GA)-4ap•DIS24(UC) kissing complex as a function of NCp7 concentration. Symbols indicating the curves for concentrations of NCp7 ranging from 75 to 500 nM are given in an inserted box. The structural isomerization rates (75 nM NCp7: $k_{conv} = 0.084 \pm 0.008$ min^{-1}; 100 nM NCp7: $k_{conv} = 0.077 \pm 0.007$ min^{-1}; 150 nM NCp7: $k_{conv} = 0.06 \pm 0.006$ min^{-1}; 250 nM NCp7: $k_{conv} = 0.460 \pm 0.024$ min^{-1}; 400 nM NCp7: $k_{conv} = 1.39 \pm 0.06$ min^{-1}; 500 nM NCp7: $k_{conv} = 2.2 \pm 0.15$ min^{-1}) were fit using a first-order rate equation. Two ranges of conversion rates are clearly observed that correspond to reactions carried out with ratios of NCp7 to DIS dimer that were either less or greater than the estimated 2:1 stoichiometry of binding.

of the DIS complex is maintained throughout the process.

In addition to probing the RNA structural rearrangement with 2-AP fluorescence, the interaction of NCp7 with the DIS stem−loops could also be monitored directly using tryptophan fluorescence (*66*, *67*) since the 55 residue NCp7 protein construct used in this study contains a single tryptophan residue. Titration of a fixed concentration of NCp7 with DIS kissing dimer results in approximately a 3-fold decrease in the NCp7 tryptophan fluorescence emission (Figure 4A) and provides a sensitive measure for the binding reaction. Using the typtophan fluorescence quenching, NCp7 is observed to bind the DIS stem−loop kissing dimer ($K_D = 61 \pm 12$ nM) with high affinity and in a saturated fashion (Figure 4A). An approximate stoichiometry of two NCp7s per one RNA dimer can also be estimated from the fluorescence binding curves, which is consistent with the C2-symmetry of the DIS dimer. While tryptophan fluorescence clearly monitors one high-affinity class of NCp7 interaction with the DIS kissing dimer, this does not exclude the possibility that additional NCp7 binding event(s) might be undetected when using tryptophan as a reporter. This could be a potential reason for why a second lower-affinity "catalytic" NCp7 binding class, which is implied by the NCp7-catalyzed DIS isomerization experiments, may not be detected by the tryptophan fluorescence measurements. NCp7 tryptophan fluorescence could also be monitored as a function of DIS conversion. In this experiment, the tryptophan fluorescence intensity at 356 nm was monitored and found to remain highly quenched during the entire course of the DIS structural isomerization (data not shown), suggesting that the high-affinity sites for NCp7 binding to the DIS kissing dimer remain occupied during the course of the structural conversion.

To further examine the ability of NCp7 to act catalytically in the DIS structural isomerization reaction, conversion rates were monitored as a function of NCp7 concentration. Under the conditions used in this experiment, DIS conversion was not observed in the absence of NCp7. Figure 4B shows fits for the rates of conversion of 100 nM DIS24(GA)-4ap•DIS24-(UC) kissing dimer as a function of increasing NCp7 concentration over a range from 75 to 500 nM. In all cases where NCp7 is added, the structural isomerization is observed to go to completion as evidenced by the common plateau of final fluorescence emission intensity. However, two distinct ranges of conversion rates are observed that correspond roughly to ratios of NCp7 to DIS kissing dimer that are either above or below the estimated 2:1 NCp7:DIS stoichiometry of high-affinity binding. An apparently maximal rate of conversion is observed when the NCp7 concentration is above the apparent 2:1 NCp7:DIS stoichiometry for high-affinity binding, while a slower average rate is observed at lower stoichiometric ratios of protein to DIS kissing dimer.

DISCUSSION

In this study, the highly fluorescent adenosine base analogue 2-AP has been selectively incorporated into RNA constructs derived from the HIV-1 DIS_{Mal} sequence to provide unambiguous and unique probes for formation of the two isoforms of the DIS_{Mal} dimer. The 2-AP fluorescence-detected equilibrium binding experiments demonstrate that truncated DIS stem−loops, which lack the wild-type stem bulge and have been altered in the loop palindromic sequence, associate under a number of experimental conditions to form kissing dimers with wild-type affinities. The formation of a kinetically stable intermediate DIS kissing dimer, however, requires the addition of divalent metal ions (Figure 5A). Thus, two different classes of the DIS kissing dimer, with distinct isomerization potentials, could be distinguished using the 2-AP fluorescence methods. The divalent metal ion-stabilized DIS kissing dimer class, which is kinetically stable, requires the addition of NCp7 to activate fast structural isomerization; while, the metastable DIS kissing dimer class, which forms with monovalent cations or at higher concentration ($>\mu$M), converts spontaneously to the mature dimer form at an appreciable but 10−20-fold slower rate than observed for NCp7.

Under all conditions tested for in vitro isomerization, the results indicate a secondary structure rearrangement mech-

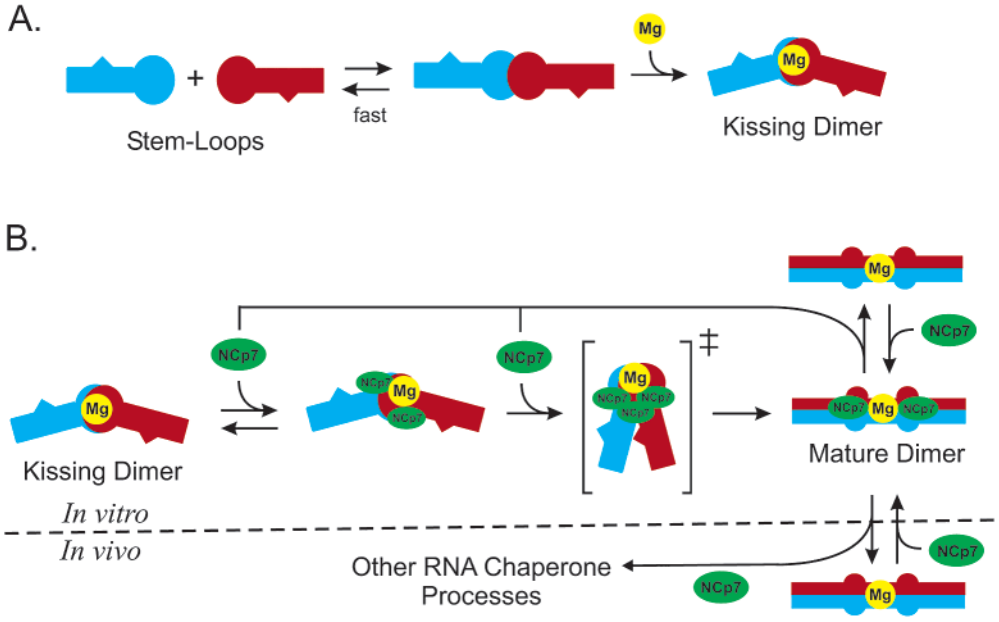

FIGURE 5: Binding pathway and proposed catalytic role of NCp7 in the structural isomerization of the DIS homodimer in vitro. (A) A collision complex initially forms via a loop−loop interaction between two individual DIS stem−loops that is stabilized by divalent metal ions. The DIS stem−loops are shown schematically in blue and red to allow them to be distinguishable from each other in the dimer complexes. The intermediate loop−loop kissing complex is kinetically trapped in the presence of Mg^{2+} (represented by a yellow sphere) and does not spontaneously convert to the mature extended duplex form. (B) NCp7 (represented by a green sphere) acts by binding to the intermediate loop−loop kissing complex in an excess of the stoichiometry of two NCp7 molecules to one DIS dimer. Binding of NCp7 decreases the energy difference between the kissing intermediate and the transition state in the refolding pathway, thereby lowering the activation energy and increasing the rate of structural isomerization. Dissociation of NCp7 from the mature extended duplex form of DIS allows it to act catalytically by rebinding and converting another intermediate kissing dimer. Since there is only one DIS interaction to act on in vivo, the biological significance of the observed recycling of NCp7 activity in vitro could be related to chaperone activities of NCp7 at different sites on the genomic RNA.

anism for isomerization that involves melting of intramolecular stem base pairs and reformation of intermolecular base pairing between the two stem helices of the DIS stem−loops. This observed mechanism is consistent with the initial proposal for in vitro DIS maturation (*16*, *29*, *30*) and results from other recent studies (*32*−*35*); however, it contradicts a recently proposed autocatalytic mechanism (*53*). On the basis of crystal structures of both kissing and extended duplex DIS dimers (*52*, *53*), Ennifar et al. argued that the nucleotides directly flanking the DIS palindromic sequence in the kissing dimer are favorably oriented for symmetrical cleavage and subsequent cross religation to produce the mature DIS dimer. If maturation proceeded through such a ribozyme-like mechanism, without melting and exchange of the stem helical strands, the stem-inserted 2-AP fluorescent probe used here would not have reported on the maturation process.

The rate enhancement observed for NCp7-activated isomerization can be rationalized in terms of the extent to which this refolding catalyst either destabilizes the kissing dimer or conversely stabilizes the transition-state folding intermediate (Figure 5B). Either type of interaction would decrease the activation energy and accelerate the rate of the DIS conversion reaction. Such a role for NCp7 would be analogous to the classic transition-state theory for how enzymes accelerate chemical reactions and suggests an enzyme-like mechanism for how this RNA chaperone functions. NCp7 is also able to turn over and affect multiple DIS conversion reactions, reinforcing the description of this RNA chaperone as a true refolding enzyme in this in vitro system (Figure 4). However, two ranges of conversion rates are observed that correspond to ratios of NCp7 to DIS kissing dimer that are either above or below the estimated 2:1 NCp7:DIS stoichiometry for high-affinity binding of NCp7. Furthermore, the apparent maximal rate for DIS isomerization is only observed when the NCp7 concentration is above the estimated 2:1 NCp7:DIS stoichiometry. These results suggest that the high-affinity sites for NCp7 binding must first be saturated before the full catalytic effect of NCp7 is observed and implies that the two NCp7 molecules occupying the high-affinity sites on DIS may be inactive in catalyzing the refolding reaction. Instead, excess "free" NCp7 may act either independently or together with the high-affinity bound NCp7 molecules in capturing and stabilizing the transition state and thereby producing the catalytic effect. Accordingly, the rate of conversion would be limited by the concentration of the free NCp7, which would depend on the off-rate of the NCp7 protein from the DIS dimers at concentrations of NCp7 that are less than the 2:1 NCp7:DIS stoichiometry of the high-affinity binding class. The off-rate of NCp7 for the DIS dimers has not been explicitly determined here; however, it can be inferred to be relatively fast from the conversion rates observed at lower stoichiometric ratios of NCp7 to DIS kissing dimer. The interpretation that the catalytic interaction of NCp7 with DIS may involve a lower-affinity, transiently bound class of molecules is also consistent with previous observations that the chaperone activity of NCp7 is not sequence specific and driven primarily through nonspecific electrostatic and intercalative interactions (*28*). It may also explain the absence of a measurable tryptophan fluorescence change for this class of NCp7 interaction.

The two apparent classes of interactions of NCp7 represented by the binding and kinetic data may indicate two unique functional roles for how NCp7 interacts with the DIS kissing dimer. NCp7's first role could involve a high-affinity

interaction with the DIS kissing dimer that results in the formation of a specific RNA−protein complex that may facilitate both DIS maturation and packaging of the genomic RNA. The second role for NCp7 would involve a transient chaperone-type interaction with the DIS kissing dimer, resulting in the destabilization of the DIS stem helices and the promotion of stem strand exchange. The description of two classes of NCp7 interaction with DIS is in some ways consistent with observations made in previous studies that a threshold concentration of approximately one NCp7 molecule per seven nucleotides of RNA is required for NCp7 to exhibit chaperone activity (*30*, *42*, *46*, *68*, *69*). In these studies, the threshold concentration of NCp7 required for demonstrable nucleic acid chaperone activity suggested that complete saturation of the RNA with NCp7 (*70*−*72*) was critical for catalytic activity and that the NCp7 chaperone activity may not turn over. The threshold concentration dependence of NCp7 activity has also lead to the proposal that interactions between NCp7 molecules bound to RNA may play a role in the chaperone effect (*73*). The results of the present study also demonstrate a threshold concentration requirement for high NCp7 activity, and this threshold concentration can be correlated with the need to first fully occupy the two high-affinity NCp7 structural binding sites on the DIS kissing dimer. Only after these binding sites are saturated is the full catalytic chaperone activity observed for the excess free NCp7. The ability of NCp7 to turn over in the DIS conversion reaction could simply reflect the limited number of available high-affinity NCp7 binding sites on the DIS kissing dimer as well as the relatively fast off-rate of NCp7 from these sites. In contrast, NCp7 may be effectively trapped as a result of the availability of a multitude of noncatalytic binding sites of moderate to high affinity in larger RNA systems (*30*, *42*, *46*, *68*, *69*) and thereby be inhibited from functioning efficiently in its role as a nucleic acid chaperone.

Furthermore, the observation of NCp7 turn over in the in vitro refolding reaction (Figure 5B) may not have specific relevance to the in vivo genome maturation process, where only a single RNA dimer exists on which NCp7 could act. Instead, the observed recycling ability of the catalytic NCp7 may function in vivo by promoting other nucleic acid structural rearrangements or transient structural binding events at other locations on the RNA strand within the budded viral particle. Alternatively, the observed turn over of NCp7 could be related to chaperone functions it may carry out as a domain within the intact *gag* protein. Since *gag* is abundant in HIV-1 infected cells and has been shown to potentate similar chaperone activities as the isolated NCp7 in vitro (*37*, *74*), the observed recycling could possibly be related to an in vivo nucleic acid chaperone function of *gag* that either requires or is made more effective by multiple turn overs in activity.

Since DIS structural isomerization can occur under different experimental conditions and requires preformation of the DIS kissing dimer, the conversion process is clearly related to the structure and dynamics of the DIS kissing dimer and is likely to involve a common transient-state RNA folding intermediate (Figure 5B). Furthermore, the structure of the Mg^{2+}-stabilized DIS kissing dimer may be preorganized to facilitate NCp7 binding and fast conversion rates. In its specific catalytic role, NCp7 accelerates the rate of strand exchange between the two hairpin stem helices without destabilization of the loop−loop helix. Under these structural constraints, NCp7 might act to facilitate the exchange of stem helices by distorting or stressing the DIS kissing conformation. One possible mode of structural distortion would be through helical bending centered on the loop−loop kissing helix, which could bring the two stem helices into close proximity and proper alignment to facilitate the isomerization process. Although not observed in the crystal structures (*52*, *53*), such a helical distortion of a kissing complex structure has precedent from previous structural studies in solution (*75*−*77*) and in this instance might uniquely involve the highly conserved purine nucleotides that flank the palindromic DIS loop sequence. These nucleotides may assume a unique conformation in the transient-state folding intermediate that both distort the DIS kissing dimer conformation and concomitantly destabilize the stem helices. In this model, the observed spontaneous conversion of the metastable DIS kissing dimers could be the result of the inherent structural plasticity in these dimers. Unlike the divalent metal ion-stabilized kissing dimer, the metastable kissing dimers might be sufficiently close in energy to the transition-state conformation such that this intermediate state is accessible through simple thermal fluctuations, and consequently spontaneous structural isomerization is possible.

In conclusion, the results of this study demonstrate a secondary structure rearrangement model for in vitro DIS stem−loop isomerization and provide insight into the role of NCp7 in catalyzing this process. How DIS structural isomerization could similarly be accomplished in vivo and how it relates to retroviral maturation and packaging still remain open questions. An isomerization mechanism involving DIS stem strand exchange, as described here for the isolated DIS hairpins, would potentially involve large-scale movements of the entire 5′ ends of the two copies of the HIV-1 RNA genome relative to each other, within the budded viral particle. Determining if and how this associated structural rearrangement could be achieved will require further studies into the molecular basis underlying the in vivo process.

ACKNOWLEDGMENT

We thank Prof. M. Summers (UMBC) for generously supplying us with a NCp7 expression plasmid, Dr. F. Song (CARB) for synthesis of the 2-AP labeled RNA oligonucleotides, and Drs. D. Brabazon and E. S. DeJong for careful reading of the manuscript.

REFERENCES

1. Paillart, J. C., Marquet, R., Skripkin, E., Ehresmann, C., and Ehresmann, B. (1996) *Biochimie 78*, 639−653.
2. Marquet, R., Paillart, J. C., Skripkin, E., Ehresmann, C., and Ehresmann, B. (1994) *Nucleic Acids Res. 22*, 145−151.
3. Laughrea, M., and Jette, L. (1994) *Biochemistry 33*, 13464−13474.
4. Miele, G., Mouland, A., Harrison, G. P., Cohen, E., and Lever, A. M. L. (1996) *J. Virol. 70*, 944−951.
5. Skripkin, E., Paillart, J. C., Marquet, R., Ehresmann, B., and Ehresmann, C. (1994) *Proc. Natl. Acad. Sci. U.S.A. 91*, 4945−4949.
6. McBride, M. S., and Panganiban, A. T. (1996) *J. Virol. 70*, 2963−2973.
7. Berkhout, B., and van Wamel, J. L. B. (1996) *J. Virol. 70*, 6723−6732.
8. Paillart, J. C., Skripkin, E., Ehresmann, B., Ehresmann, C., and Marquet, R. (1996) *Proc. Natl. Acad. Sci. U.S.A. 93*, 5572−5577.

9. Clever, J. L., and Parslow, T. G. (1997) *J. Virol. 71*, 3407−3414.
10. Laughrea, M., Jette, L., Mak, J., Kleiman, L., Liang, C., and Wainberg, M. A. (1997) *J. Virol. 71*, 3397−3406.
11. Laughrea, M., Shen, N., Jette, L., and Wainberg, M. A. (1999) *Biochemistry 38*, 226−234.
12. Muriaux, D., Girard, P. M., Bonnetmathoniere, B., and Paoletti, J. (1995) *J. Biol. Chem. 270*, 8209−8216.
13. Clever, J. L., Wong, M. L., and Parslow, T. G. (1996) *J. Virol. 70*, 5902−5908.
14. Haddrick, M., Lear, A. L., Cann, A. J., and Heaphy, S. (1996) *J. Mol. Biol. 259*, 58−68.
15. Laughrea, M., and Jette, L. (1996) *Biochemistry 35*, 9366−9374.
16. Laughrea, M., and Jette, L. (1996) *Biochemistry 35*, 1589−1598.
17. Paillart, J. C., Berthoux, L., Ottmann, M., Darlix, J. L., Marquet, R., Ehresmann, B., and Ehresmann, C. (1996) *J. Virol. 70*, 8348−8354.
18. Shen, N., Jette, L., Liang, C., Wainberg, M. A., and Laughrea, M. (2000) *J. Virol. 74*, 5729−5735.
19. Skripkin, E., Paillart, J. C., Marquet, R., Blumenfeld, M., Ehresmann, B., and Ehresmann, C. (1996) *J. Biol. Chem. 271*, 28812−28817.
20. Paillart, J.-C., Marquet, R., Skripkin, E., Ehresmann, B., and Ehresmann, C. (1994) *J. Biol. Chem. 269*, 27486−27493.
21. Paillart, J.-C., Westhof, E., Ehresmann, C., Ehresmann, B., and Marquet, R. (1997) *J. Mol. Biol. 270*, 36−49.
22. Lodmell, J. S., Paillart, J. C., Mignot, D., Ehresmann, B., Ehresmann, C., and Marquet, R. (1998) *Antisense Nucleic Acid Drug Dev. 8*, 517−529.
23. Jossinet, F., Paillart, J. C., Westhof, E., Hermann, T., Skripkin, E., Lodmell, J. S., Ehresmann, C., Ehresmann, B., and Marquet, R. (1999) *RNA 5*, 1222−1234.
24. Lodmell, J. S., Ehresmann, C., Ehresmann, B., and Marquet, R. (2000) *RNA 6*, 1267−1276.
25. Lodmell, J. S., Ehresmann, C., Ehresmann, B., and Marquet, R. (2001) *J. Mol. Biol. 311*, 475−490.
26. Fu, W., and Rein, A. (1993) *J. Virol. 67*, 5443−5449.
27. Fu, W., Gorelick, R. J., and Rein, A. (1994) *J. Virol. 68*, 5013−5018.
28. Rein, A., Henderson, L. E., and Levin, J. G. (1998) *Trends Biochem. Sci. 23*, 297−301.
29. Muriaux, D., DeRocquigny, H., Roques, B. P., and Paoletti, J. (1996) *J. Biol. Chem. 271*, 33686−33692.
30. Feng, Y. X., Copeland, T. D., Henderson, L. E., Gorelick, R. J., Bosche, W. J., Levin, J. G., and Rein, A. (1996) *Proc. Natl. Acad. Sci. U.S.A. 93*, 7577−7581.
31. Muriaux, D., Fosse, P., and Paoletti, J. (1996) *Biochemistry 35*, 5075−5082.
32. Theilleux-Delalande, V., Girard, F., Huynh-Dinh, T., Lancelot, G., and Paoletti, J. (2000) *Eur. J. Biochem. 267*, 2711−2719.
33. Takahashi, K. I., Baba, S., Chattopadhyay, P., Koyanagi, Y., Yamamoto, N., Takaku, H., and Kawai, G. (2000) *RNA 6*, 96−102.
34. Takahashi, K., Baba, S., Koyanagi, Y., Yamamoto, N., Takaku, H., and Kawai, G. (2001) *J. Biol. Chem. 276*, 31274−31278.
35. Huthoff, H., and Berkhout, B. (2002) *Biochemistry 41*, 10439−10445.
36. Remy, E., de Rocquigny, H., Petitjean, P., Muriaux, D., Theilleux, V., Paoletti, J., and Roques, B. P. (1998) *J. Biol. Chem. 273*, 4819−4822.
37. Feng, Y. X., Campbell, S., Harvin, D., Ehresmann, B., Ehresmann, C., and Rein, A. (1999) *J. Virol. 73*, 4251−4256.
38. Chan, B. D., Weidemaier, K., Yip, W. T., Barbara, P. F., and Musier-Forsyth, K. (1999) *Proc. Natl. Acad. Sci. U.S.A. 96*, 459−464.
39. Peliska, J. A., Balasubramanian, S., Giedroc, D. P., and Benkovic, S. J. (1994) *Biochemistry 33*, 13817−13823.
40. Li, X. G., Quan, Y. D., Arts, E. J., Li, Z., Preston, B. D., deRocquigny, H., Roques, B. P., Darlix, J. L., Kleiman, L., Parniak, M. A., and Wainberg, M. A. (1996) *J. Virol. 70*, 4996−5004.
41. Wu, T. Y., Guo, J. H., Bess, J., Henderson, L. E., and Levin, J. G. (1999) *J. Virol. 73*, 4794−4805.
42. Wu, W. X., Henderson, L. E., Copeland, T. D., Gorelick, R. J., Bosche, W. J., Rein, A., and Levin, J. G. (1996) *J. Virol. 70*, 7132−7142.
43. Johnson, P. E., Turner, R. B., Wu, Z. R., Hairston, L., Guo, J. H., Levin, J. G., and Summers, M. F. (2000) *Biochemistry 39*, 9084−9091.
44. Guo, J. H., Wu, T. Y., Kane, B. F., Johnson, D. G., Henderson, L. E., Gorelick, R. J., and Levin, J. G. (2002) *J. Virol. 76*, 4370−4378.
45. Guo, J. H., Wu, T. Y., Anderson, J., Kane, B. F., Johnson, D. G., Gorelick, R. J., Henderson, L. E., and Levin, J. G. (2000) *J. Virol. 74*, 8980−8988.
46. Guo, J. H., Henderson, L. E., Bess, J., Kane, B., and Levin, J. G. (1997) *J. Virol. 71*, 5178−5188.
47. Williams, M. C., Gorelick, R. J., and Musier-Forsyth, K. (2002) *Proc. Natl. Acad. Sci. U.S.A. 99*, 8614−8619.
48. Urbaneja, M. A., Wu, M., Casas-Finet, J. R., and Karpel, R. L. (2002) *J. Mol. Biol. 318*, 749−764.
49. Mujeeb, A., Clever, J. L., Billeci, T. M., James, T. L., and Parslow, T. G. (1998) *Nat. Struct. Biol. 5*, 432−436.
50. Girard, F., Barbault, F., Gouyette, C., Huynh-Dinh, T., Paoletti, J., and Lancelot, G. (1999) *J. Biomol. Struct. Dyn. 16*, 1145−1157.
51. Mujeeb, A., Parslow, T. G., Zarrinpar, A., Das, C., and James, T. L. (1999) *FEBS Lett. 458*, 387−392.
52. Ennifar, E., Yusupov, M., Walter, P., Marquet, R., Ehresmann, B., Ehresmann, C., and Dumas, P. (1999) *Struct. Fold. Des. 7*, 1439−1449.
53. Ennifar, E., Walter, P., Ehresmann, B., Ehresmann, C., and Dumas, P. (2001) *Nat. Struct. Biol. 8*, 1064−1068.
54. Lacourciere, K. A., Stivers, J. T., and Marino, J. P. (2000) *Biochemistry 39*, 5630−5641.
55. Parrott, A., Lago, H., Adoms, C., Ashcroft, A., Stonehouse, N., and Stockley, P. (2000) *Nucleic Acids Res. 28*, 489−497.
56. Menger, M., Tuschl, T., Eckstein, F., and Porschke, D. (1996) *Biochemistry 35*, 14710−14716.
57. Menger, M., Eckstein, F., and Porschke, D. (2000) *Nucleic Acids Res. 28*, 4428−4434.
58. Rist, M. J., and Marino, J. P. (2001) *Nucleic Acids Res. 29*, 2401−2408.
59. Beaucage, S. L., and Caruthers, M. H. (1981) *Tetrahedron Lett. 22*, 1859.
60. Milligan, J. F., and Uhlenbeck, O. C. (1989) *Methods Enzymol. 180*, 51.
61. Milligan, J. F., Groebe, D. R., Witherell, G. W., and Uhlenbeck, O. C. (1987) *Nucleic Acids Res. 15*, 8783−8798.
62. Amarasinghe, G. K., De Guzman, R. N., Turner, R. B., Chancellor, K. J., Wu, Z. R., and Summers, M. F. (2000) *J. Mol. Biol. 301*, 491−511.
63. Eguchi, Y., Itoh, T., and Tomizawa, J. (1991) *Annu. Rev. Biochem. 60*, 631−652.
64. Wagner, E. G. H., and Simons, R. W. (1994) *Annu. Rev. Microbiol. 48*, 712−42.
65. Mely, Y., Stoylov, S. P., Vuilleumier, C., Roques, B. P., and Gerard, D. (1996) *Prog. Biophys. Mol. Biol. 65*, PB203.
66. Vuilleumier, C., Bombarda, E., Morellet, N., Gerard, D., Roques, B. P., and Mely, Y. (1999) *Biochemistry 38*, 16816−16825.
67. Bombarda, E., Ababou, A., Vuilleumier, C., Gerard, D., Roques, B. P., Piemont, E., and Mely, Y. (1999) *Biophys. J. 76*, 1561−1570.
68. Khan, R., and Giedroc, D. P. (1992) *J. Biol. Chem. 267*, 6689−6695.
69. You, J. C., and McHenry, C. S. (1994) *J. Biol. Chem. 269*, 31491−31495.
70. Karpel, R. L., Henderson, L. E., and Oroszlan, S. (1987) *J. Biol. Chem. 262*, 4961−4967.
71. Dibhajj, F., Khan, R., and Giedroc, D. P. (1993) *Protein Sci. 2*, 231−243.
72. You, J. C., and McHenry, C. S. (1993) *J. Biol. Chem. 268*, 16519−16527.
73. Tanchou, V., Gabus, C., Rogemond, V., and Darlix, J. L. (1995) *J. Mol. Biol. 252*, 563−571.
74. Berkowitz, R. D., Ohagen, A., Hoglund, S., and Goff, S. P. (1995) *J. Virol. 69*, 6445−6456.
75. Marino, J. P., Gregorian, R. S., Csankovszki, G., and Crothers, D. M. (1995) *Science 268*, 1448−1454.
76. Lee, A., and Crothers, D. (1998) *Structure 6*, 993−1005.
77. Chang, K.-Y., and Tinoco, I. (1997) *J. Mol. Biol. 269*, 52−66.

BI0267240